

# Optimal Operation of an Integrated Electricity-heat Energy System Considering Flexible Resources Dispatch for Renewable Integration

Wei Wang, Shuhao Huang, Guangming Zhang, Jizhen Liu, and Zhe Chen, *IEEE, Fellow*

**Abstract**—Large fluctuations may occur on the energy supply and the load sides when large-scale renewable energies are integrated, leading to great challenges in power systems. The renewable power curtailment is especially numerous in the integrated electricity-heat energy system (IEHES) on account of electricity-heat coupling. The flexible resources (FRs) on both the energy supply and load sides are introduced into the optimal dispatch of the IEHES and further modeled to alleviate the renewable fluctuations in this paper. On the energy supply side, three kinds of FRs based on electricity-heat coordination are modeled and discussed. On the load side, the shiftable electricity demand resource is characterized. On this basis, the solution for FRs participating in IEHES dispatch is given, with goals of maximizing the renewable penetration ratio and lowering operation costs. Two scenarios are performed, and the results indicate that the proposed optimal dispatch strategy can effectively reduce the renewable energy curtailment and improve the flexibility of the IEHES. The contribution degrees of different FRs for renewable integration are also explored.

**Index Terms**—Integrated electricity-heat energy system (IEHES), renewable penetration, flexible resource (FR), electricity-heat coordination, shiftable demand load.

## I. INTRODUCTION

IN recent years, renewable energy has received increasing attention from all over the world due to the deterioration of the ecological environment and the energy shortage crisis [1], [2]. In China, the government has been actively promoting the construction of wind power and photovoltaic projects. As of September 2020, China's installed renewable energy power generation capacity has reached 837 million kW, of which wind power and photovoltaic power generation are

nearly 223 million kW [3]. However, the rapid development of renewable energy brings some problems to the integrated energy system [4]. In the first three quarters of 2020, the curtailment of wind and photovoltaic powers in China reached 11.6 and 3.43 billion kWh, respectively, mainly in the Three Norths Region (referring to Northeast, North, and Northwest China).

This phenomenon can be attributed to the strong random volatility and intermittence of wind power and photovoltaics [5]. When the large-scale renewable energy is connected to the power grid, both the power and load sides fluctuate randomly, making the stable operation of the power system challenging. If the flexible resources (FRs) are not enough for system dispatch, the renewable energy with weak controllability is discarded [6]. This situation is especially aggravated in an integrated electricity-heat energy system (IEHES) because many combined heat and power (CHP) units are operated in the heat-led mode, and the electricity outputs are heavily restricted by heat production [7], [8]. Decoupling electricity and heat productions and the appropriate use of shiftable demand load have been proven efficient to improve the operation flexibility of power system.

Many researches have been carried out on electricity-heat coordination techniques. On CHP units, [9] proposes to configure energy storage equipment to alleviate the coupling constraints of electricity and heat. Reference [10] verifies the great potential of heat pumps and electric immersion boilers in improving the flexibility of the energy system in Copenhagen, Denmark. Reference [11] evaluates the potential benefits of applying pumped water storage and electric boilers (EBs) to the western region of Inner Mongolia. Reference [12] introduces a phase change heat storage device (HSD) into the CHP system and improves the operation flexibility of power system. Reference [13] studies the internal heat exchange model of the solid heat storage boiler and applies it to the optimal dispatch of the CHP system. Reference [14] proposes an optimal economic dispatch model of the CHP system including an EB and a thermal storage tank. Furthermore, the thermal inertia of district heating system (DHS) has been discussed. Reference [15] formulates a CHP dispatch considering the temperature dynamics of the district heating network (DHN) for managing the variability of wind energy. Reference [16] models the heat storage capacity of the DHN by capturing the quasi-dynamic characteristics of

Manuscript received: December 29, 2020; accepted: June 23, 2021. Date of CrossCheck: June 23, 2021. Date of online publication: July 30, 2021.

This work was supported by the National Natural Science Foundation of China (No. 52076073).

This article is distributed under the terms of the Creative Commons Attribution 4.0 International License (<http://creativecommons.org/licenses/by/4.0/>).

W. Wang (corresponding author) and J. Liu are with the State Key Laboratory of Alternate Electrical Power System with Renewable Energy Sources, North China Electric Power University, Beijing 102206, China (e-mail: wwang@ncepu.edu.cn; ljz@ncepu.edu.cn).

S. Huang and G. Zhang are with the School of Control and Computer Engineering, North China Electric Power University, Beijing 102206, China (e-mail: 2358173023@qq.com; gm\_zhang@outlook.com).

Z. Chen is with the Department of Energy Technology, Aalborg University, 9220 Aalborg, Denmark (e-mail: zch@et.aau.dk).

DOI: 10.35833/MPCE.2020.000917



pipeline temperature. Reference [17] analyzes a decentralized solution to the coordinated dispatch of integrated systems and formulates a convex coordination model considering the pipeline energy storage. Reference [18] configures the pipeline heat storage in a CHP dispatch model under the constant mass flow heating dispatch mode. In [19], the integration of wind power is enhanced by using the free heat storage of the primary DHN and introducing extra heat pumps. Reference [20] proposes an optimal system scheduling strategy that comprehensively considers the operation mode of the district heating pipe network and the heat storage capacity of the building. In [21], a complete hydraulic and dynamic thermal model of the indirect connection district heating system is proposed to simulate the dynamic temperature distribution. In the integrated electric heating dispatching system established in [22]-[25], the thermal inertia and comfort on the demand side of the DHS are analyzed and modeled. References [26]-[29] analyze the heat transfer process of the DHN, equivalent buildings, and the thermal energy storage in the CHP system, and propose an iteration solution to deal with such non-linear heat transfer constraints. Reference [30] introduces a novel market framework based on a hierarchical optimization model to achieve the coordination of electricity-heat systems, and develops an augmented regularized Benders decomposition algorithm. Reference [31] uses the stochastic fractal search optimization technique to treat the highly non-linear CHP economic dispatch problem. Reference [32] presents a mixed-integer linear programming (MILP) model for the microgrid optimal scheduling and different energy converters or storages are considered.

On the load side, demand response (DR) has been widely used to provide support for power system stability. Reference [33] analyzes the effect of market structure on the elasticity of the demand for electricity and then describes how the behavior of consumers can be modeled using a matrix of elasticities. Reference [34] proposes the basic concept of DR and provides a comprehensive theoretical explanation in conjunction with the IEHES market. Reference [35] establishes a method of accommodating both wind power and DR uncertainties and verifies that DR can help accommodate the wind power output uncertainty by lowering the unit load cost. In [36], the price-based DR (PDR) and incentive-based DR (IDR) are introduced to build the DR model and improve the wind power consumption capability of the system.

All the above researches have improved the operation flexibility of the electric power system (EPS) to a certain degree. However, the orderly classification and modeling for FRs and their contribution degrees for renewable penetration are seldom discussed. And the optimization solution for various FRs participating in IEHES dispatch is rarely mentioned in the literature. The contributions of this paper are described as follows. Firstly, different FRs are orderly classified and modeled for renewable penetration. Secondly, the solution for FRs participating in IEHES dispatch is given, with the goals of maximizing the renewable penetration ratio and lowering operation costs. Thirdly, the contribution degrees of different FRs for renewable integration are explored.

The remainder of this paper is organized as follows. Section II presents the detailed modeling and analysis of FRs in an IEHES. Section III presents the electricity-heat dispatch problem and solution in an IEHES. Section IV discusses cases that verify the effectivity of the proposed method. Section V provides the conclusion.

## II. MODELING FOR FRs

This paper studies an IEHES, which contains two subsystems, i.e., the EPS and the DHS, as shown in Fig. 1. The EPS prefers real-time energy balance for system stability and electricity quality. However, an IEHES commonly operates in a heat-led mode, which seriously restricts the dispatch of EPS. Meanwhile, DHS is not very demanding on real-time performance because of the heat delay and inertia, and its heat production has complementary characteristics with electricity production, i.e., electricity is easy to transfer but difficult to store in large scale, whereas heat production is difficult to transfer but easy to store. Consequently, improving the operation flexibility of EPS through heat and electricity decoupling has great potential. Furthermore, reducing the fluctuations on the load side greatly contributes to the flexibility of EPS. The above approaches can both be classified into FRs, which play a decisive role in renewable penetration for a fixed EPS.

Various technologies and methods that can promote the renewable penetration are introduced above such as heat pumps, EBs, and thermal inertia of heating pipe networks. Considering practicality and feasibility, two types of FRs are focused on in this paper. The first type is electricity-heat coordination resources (EHCRs), which contain the electricity decoupled by the HSD, the electricity decoupled by the heat storage in DHN, and the convertible electricity from the EB. The second one belongs to the load side and is called shiftable electricity demand resource (SEDR). The characteristics and models of the mentioned FRs are presented below.

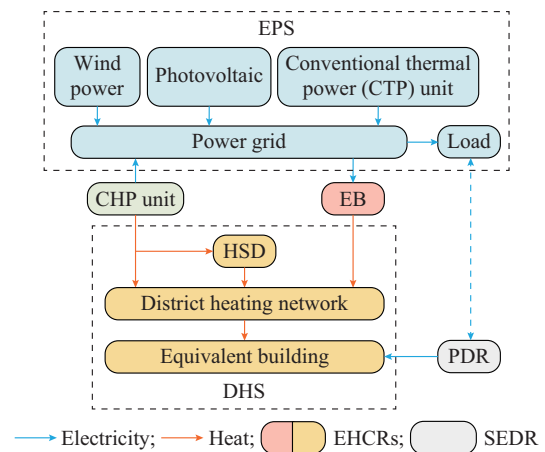


Fig. 1. Schematic of IEHES.

### A. EHCRs

#### 1) Electricity Released by HSD

An HSD stores heat from CHP units when the electricity demand is greater than the electricity productions under the

rated heating supply condition. The heat storage in the HSD compensates for the lack of heating from the CHP units when their electricity productions are limited. The heat storage capacity of the HSD determines the released electricity quantity. The constraints of heat storage and release power can be expressed as:

$$0 \leq H_{i,t}^{st} \leq H_{i,t}^{st,max} \quad (1)$$

$$0 \leq H_{i,t}^{rl} \leq H_{i,t}^{rl,max} \quad (2)$$

$$H_{i,t}^{st} H_{i,t}^{rl} = 0 \quad (3)$$

where  $H_{i,t}^{st}$  and  $H_{i,t}^{rl}$  are the heat storage and release power of HSD  $i$  at time  $t$ , respectively; and  $H_{i,t}^{st,max}$  and  $H_{i,t}^{rl,max}$  are the maximum heat storage and release power of HSD  $i$ , respectively. Moreover, the heat storage and release cannot occur simultaneously.

The constraints of heat storage are expressed as:

$$S_{i,t}^{HSD} = S_{i,t-1}^{HSD} + (H_{i,t}^{st} - H_{i,t}^{rl} - H_{i,t}^{HSD,loss})\Delta t \quad (4)$$

$$H_{i,t}^{HSD,loss} = k_i^{HSD,loss} S_{i,t}^{HSD} \quad (5)$$

$$0 \leq S_{i,t}^{HSD} \leq S_{i,t}^{HSD,max} \quad (6)$$

$$S_{i,0}^{HSD} = S_{i,N}^{HSD} \quad (7)$$

where  $S_{i,t}^{HSD}$  is the heat storage of HSD  $i$  at time  $t$ ;  $S_{i,t}^{HSD,max}$  is the upper limit of  $S_{i,t}^{HSD}$ ;  $H_{i,t}^{HSD,loss}$  is the energy loss;  $\Delta t$  is the time interval; and  $k_i^{HSD,loss}$  is the heat loss coefficient. In addition, the heat storage at the last time is equal to that at the initial time.

As shown in Fig. 2, the original feasible area of the CHP unit is within A-B-C-D. After configuring the HSD, lines AB and BC shift to the right, and line CD shifts to the left. The operation area expands to A-E-F-G-H-I. The electric power adjustment range corresponding to reference heat power  $H_{ref}$  expands from  $(P_2, P_1)$  to  $(P_4, P_3)$ , indicating that the HSD can alleviate the severe electrothermal coupling of the CHP unit and improve the scheduling flexibility of IEHES.

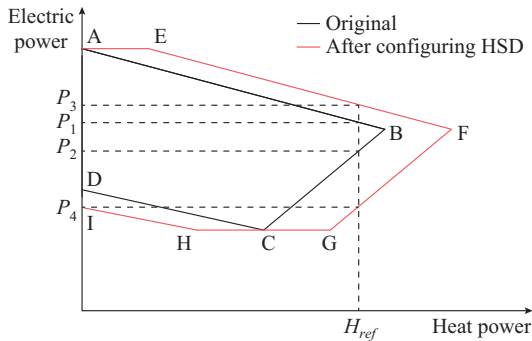


Fig. 2. Electrothermal coupling characteristics of CHP unit with HSD.

## 2) Electricity Released by Heat Storage in DHN

### 1) Storage in DHN pipeline

The pipeline structure of the DHN is shown in Fig. 3. The heat provided by the heat source enters the building through the primary heating network (PHN) and the secondary heating network (SHN):

$$H_t^{hs} = (T_t^{PHN,out} - T_t^{PHN,in})m^{PHN}c^{water} \quad (8)$$

$$H_{i,t}^{br} = (T_{i,t}^{br,in} - T_{i,t}^{br,out})m_{i,t}^{br}c^{water} \quad (9)$$

where  $H_t^{hs}$  is the total heat input from the heat source at time  $t$ ;  $T_t^{PHN,in}$  and  $T_t^{PHN,out}$  are the inlet and outlet water temperatures of the PHN, respectively;  $m^{PHN}$  and  $c^{water}$  are the mass flow rate and specific heat capacity of water in the PHN main pipeline, respectively;  $H_{i,t}^{br}$  is the heat power transfer from the PHN to SHN  $i$  at time  $t$ ;  $T_{i,t}^{br,in}$  and  $T_{i,t}^{br,out}$  are the inlet and outlet temperatures of PHN branch pipeline  $i$  at time  $t$ , respectively; and  $m_{i,t}^{br}$  is the mass flow rate of PHN branch pipeline  $i$  at time  $t$ .

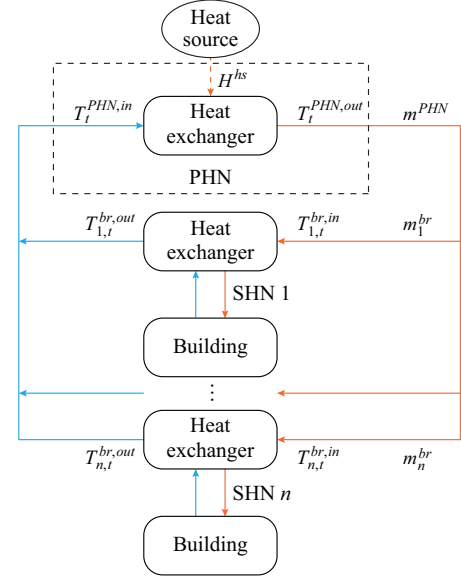


Fig. 3. Schematic of DHN pipeline connection.

The pipeline transmission time delay causes thermal inertia. The pipeline length of the PHN can reach several kilometers, so we can use a considerable amount of water in the pipeline to store or release heat. Figure 4 shows the passive heat storage and release processes of the PHN.  $T_{ref}^{PHN,in}$  and  $T_{ref}^{PHN,out}$  are the inlet and outlet reference water temperatures of the PHN, respectively.  $\Delta T_{ref}$  is the difference between the outlet and inlet water temperatures. Areas A, B, and C reflect the time delay of the outlet and inlet water temperature changes. Among them, A and C reflect the heat storage capacity, while B reflects the heat release capacity.

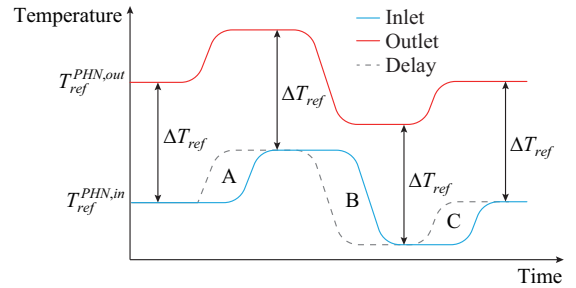


Fig. 4. Thermal inertia of PHN.

### 2) Storage in building

The thermodynamic model of the equivalent building is introduced in [37]-[39], which we simplify into a first-order equivalent thermal parameter model:

$$H_{i,t}^{br} = C_i^b (T_{i,t}^b - T_{i,t-1}^b) + H_{i,t}^{b,loss} \quad (10)$$

$$H_{i,t}^{b,loss} = \frac{T_{i,t}^b - T_i^{env}}{R_i^b} \quad (11)$$

where  $T_{i,t}^b$  is the indoor temperature of equivalent building  $i$  at time  $t$ ;  $T_i^{env}$  is the outside environment temperature;  $C_i^b$  and  $R_i^b$  are the thermal capacity and resistance of building  $i$ , respectively; and  $H_{i,t}^{b,loss}$  is the heat lost to the outside environment of building  $i$  at time  $t$ . Part of the heat from the SHN is stored inside the building envelopes. The other part is lost to the external environment to maintain the indoor temperature.

As shown in Fig. 5, the change in indoor temperature  $T_{i,t}^b$  reflects the thermal inertia of the equivalent building.  $T_{i,t}^{b,max}$  and  $T_{i,t}^{b,min}$  are the upper and lower limits of the indoor temperature acceptable to the users, respectively.  $T_{i,t}^{b,ref}$  is the reference indoor temperature without considering the heat storage capacity. Compared with  $T_{i,t}^{b,ref}$ , the decrease of  $T_{i,t}^b$  reflects the state of heat storage, while the increase of  $T_{i,t}^b$  reflects the state of heat release.



Fig. 5. Thermal inertia of equivalent building.

The thermal inertia of the PHN and equivalent buildings reflects the passive heat storage capacity of the DHS, which can adjust the heat load of the CHP unit, thereby indirectly alleviating the serious thermoelectric coupling and improving the scheduling flexibility of the IEHES.

### 3) Convertible Electricity by EB

EBs can convert electricity into heat power for the heating demand when the electricity productions are excessive. For direct heating EBs, the electricity from the EPS is directly converted to heat and sent to the DHS, thereby realizing energy conversion in the system. The electricity consumption is linearly related to the heat putout:

$$H_{i,t}^{EB} = k_i^{EB} P_{i,t}^{EB} \quad (12)$$

$$0 \leq P_{i,t}^{EB} \leq P_i^{EB,max} \quad (13)$$

$$0 \leq H_{i,t}^{EB} \leq H_i^{EB,max} \quad (14)$$

where  $P_{i,t}^{EB}$  and  $H_{i,t}^{EB}$  are the electric power input and heat power output of EB  $i$  at time  $t$ , respectively;  $k_i^{EB}$  is the conversion coefficient of EB  $i$ ; and  $P_i^{EB,max}$  and  $H_i^{EB,max}$  are the upper limits of the electric and heat power outputs, respectively.

EBs are usually installed near the CHP unit as a heat source. The electrothermal coupling characteristics of the CHP unit with the EB is shown in Fig. 6. The original feasible area of the CHP unit is within A-B-C-D. After adding the EB, lines BC and CD move to the lower right. The oper-

ation area expands to A-B-E-F-G-D. The dispatch range of electric power as for the reference heat power is expanded from  $(P_2, P_1)$  to  $(P_3, P_1)$ , indicating that the installation of the electricity-to-heat (E2H) resource is an efficient way of decoupling the electricity and heat productions for improving the operation flexibility of the EPS.

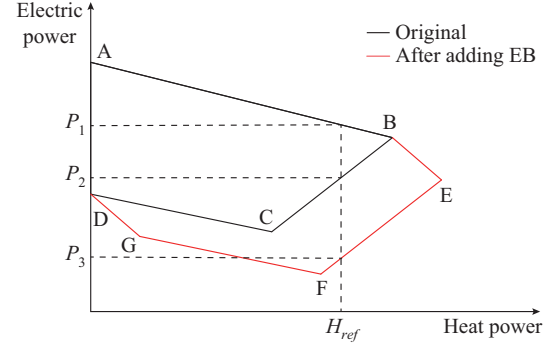


Fig. 6. Electrothermal coupling characteristics of CHP unit with EB.

### B. SEDR

The orderly utilization of SEDR can reduce the electricity demand fluctuations and promote the renewable penetration. PDR is an efficient approach to motivating electricity consumers to participate in DR.

The load change rate  $k^{el}$  and electricity price change rate  $k^{pr}$  are expressed as:

$$k^{el} = \frac{Q^{el}}{P^{el}} \quad (15)$$

$$k^{pr} = \frac{Q^{pr}}{P^{pr}} \quad (16)$$

where  $Q^{el}$  is the electricity load change;  $P^{el}$  is the original value of electricity;  $Q^{pr}$  is the electricity price change; and  $P^{pr}$  is the original electricity price.

In economics, the relationship between price and load change rates is expressed as:

$$k_i^{el} = e_{ii} k_i^{pr} \quad (17)$$

$$k_j^{el} = e_{ij} k_j^{pr} \quad (18)$$

where  $e_{ii}$  and  $e_{ij}$  are the respective self-elastic and mutual-elastic coefficients of electricity and price, respectively, which represent the load DR to the electricity prices in current period  $i$  or another period  $j$ .

We use the elasticity matrix to describe the load DR to electricity prices in multiple periods:

$$\begin{bmatrix} k_1^{el} \\ k_2^{el} \\ \vdots \\ k_T^{el} \end{bmatrix} = \mathbf{E} \begin{bmatrix} k_1^{pr} \\ k_2^{pr} \\ \vdots \\ k_T^{pr} \end{bmatrix} = \begin{bmatrix} e_{11} & e_{12} & \cdots & e_{1T} \\ e_{21} & e_{22} & \cdots & e_{2T} \\ \vdots & \vdots & \ddots & \vdots \\ e_{T1} & e_{T2} & \cdots & e_{TT} \end{bmatrix} \begin{bmatrix} k_1^{pr} \\ k_2^{pr} \\ \vdots \\ k_T^{pr} \end{bmatrix} \quad (19)$$

where  $T$  is the scheduling period; and  $\mathbf{E}$  is the price-based demand elasticity matrix, in which the main diagonal is the self-elasticity coefficient, and the sub-diagonal is the mutual elasticity coefficient.

Considering the consumer satisfaction constraints, the electricity consumption satisfaction index is introduced to ensure that the electric load change is controlled within an accept-

able range:

$$Sat = 1 - \frac{\sum_{t=1}^T |Q_t^{el}|}{\sum_{t=1}^T P^{el}} \quad (20)$$

$$Sat \geq Sat^{\min} \quad (21)$$

where  $Sat$  is the electricity consumption satisfaction index; and  $Sat^{\min}$  is the lower limit of  $Sat$ .

The sum of load changes in the entire scheduling period is zero, so the total load demand remains unchanged:

$$\sum_{t=1}^T Q_t^{el} = 0 \quad (22)$$

The electricity price change at each time is limited to prevent excessive fluctuations:

$$|Q_t^{pr}| \leq Q^{pr, \lim} \quad (23)$$

By adjusting the electricity price to change the load demand, we can improve the integration of renewable energy and the flexibility of the IEHES.

### III. OPTIMAL DISPATCH OF IEHES

#### A. Objective Function

The objective of IEHES dispatch is to minimize the total cost:

$$C^{total} = \min(C^{CHP} + C^{CTP} + C^{WP} + C^{PV}) \quad (24)$$

where  $C^{total}$  is the total cost;  $C^{CHP}$  and  $C^{CTP}$  are the costs of coal consumption of the CHP and CTP units, respectively; and  $C^{WP}$  and  $C^{PV}$  are the curtailment penalty costs of wind power and photovoltaics, respectively.

The total cost  $C^{total}$  consists of the unit operation and renewable energy curtailment costs. The purpose of adding renewable energy curtailment costs is to increase the renewable penetration. The penalty function is expressed as:

$$C^{WP} = k^{WP} (P^{WP, av} - P^{WP}) \quad (25)$$

$$C^{PV} = k^{PV} (P^{PV, av} - P^{PV}) \quad (26)$$

where  $P^{WP, av}$  and  $P^{WP}$  are the forecasting and actual values of wind power output, respectively;  $P^{PV, av}$  and  $P^{PV}$  are the forecasting and actual value of photovoltaic output, respectively; and  $k^{WP}$  and  $k^{PV}$  are the penalty factors.

The operation costs of CHP and CTP units can be expressed as a quadratic function of unit output:

$$C^{CHP} = k_1^{CHP} + k_2^{CHP} P^{CHP} + k_3^{CHP} m^{CHP} + k_4^{CHP} (P^{CHP})^2 + k_5^{CHP} (m^{CHP})^2 + k_6^{CHP} P^{CHP} m^{CHP} \quad (27)$$

$$C^{CTP} = k_1^{CTP} (P^{CTP})^2 + k_2^{CTP} P^{CTP} + k_3^{CTP} \quad (28)$$

where  $k_1^{CHP}$  and  $k_2^{CTP}$  are the cost coefficients of the CHP and CTP units, respectively;  $P^{CHP}$  and  $m^{CHP}$  are the electric power output and the extraction steam mass flow of CHP units, respectively; and  $P^{CTP}$  is the electric power output of CTP units.

#### B. System Constraints

##### 1) EPS

The electric power and heat source flow of CHP unit can

be formulated by a convex combination of extreme points [9]:

$$P_{i,t}^{CHP} = \sum_{k=1}^{M_i} p_i^k x_{i,t}^k \quad (29)$$

$$m_{i,t}^{CHP} = \sum_{k=1}^{M_i} m_i^k x_{i,t}^k \quad (30)$$

$$\begin{cases} \sum_{k=1}^{M_i} x_{i,t}^k = 1 \\ 0 \leq x_{i,t}^k \leq 1 \end{cases} \quad \forall i \in I^{CHP}, \forall t \in T \quad (31)$$

where  $I^{CHP}$  is the index set of the CHP units;  $P_{i,t}^{CHP}$  is the electric power output of CHP unit  $i$  at time  $t$ ;  $m_{i,t}^{CHP}$  is the extraction steam mass flow of CHP unit  $i$  at time  $t$ ;  $M_i$  is the total number of extreme points of the feasible operation area;  $x_{i,t}^k$  is the combination coefficient of extreme point  $k$  for CHP unit  $i$  at time  $t$ ; and  $p_i^k$  and  $m_i^k$  are the electric power and extraction steam mass flow of corner point  $k$  of CHP unit  $i$ , respectively.

The power output of the CTP units is constrained by their generation capacity:

$$P_i^{CTP, \min} \leq P_{i,t}^{CTP} \leq P_i^{CTP, \max} \quad (32)$$

where  $P_{i,t}^{CTP}$  is the electric power of CTP unit  $i$  at time  $t$ ; and  $P_i^{CTP, \max}$  and  $P_i^{CTP, \min}$  are the upper and lower limits of  $P_{i,t}^{CTP}$ , respectively.

The CTP and CHP units have ramping constraints in two adjacent scheduling intervals:

$$-P_i^{CTP, r} \leq \frac{P_{i,t+1}^{CTP} - P_{i,t}^{CTP}}{\Delta t} \leq P_i^{CTP, r} \quad (33)$$

$$-P_i^{CHP, r} \leq \frac{P_{i,t+1}^{CHP} - P_{i,t}^{CHP}}{\Delta t} \leq P_i^{CHP, r} \quad (34)$$

where  $P_i^{CTP, r}$  and  $P_i^{CHP, r}$  are the ramping capacities of the CTP and CHP units, respectively; and  $\Delta t$  is the time interval.

The actual power outputs of wind turbines and photovoltaic units should be limited by the predicted available power:

$$0 \leq P_{i,t}^{WP} \leq P_{i,t}^{WP, av} \quad (35)$$

$$0 \leq P_{i,t}^{PV} \leq P_{i,t}^{PV, av} \quad (36)$$

where  $P_{i,t}^{WP}$  and  $P_{i,t}^{PV}$  are the actual power outputs of wind turbine  $i$  and photovoltaic unit  $i$  at time  $t$ , respectively; and  $P_{i,t}^{WP, av}$  and  $P_{i,t}^{PV, av}$  are the predicted available powers.

The transmission lines of the EPS have power flow constraints. The transmission power of each branch should not exceed its limit:

$$-P_l^{br, \lim} \leq P_{l,t}^{br} \leq P_l^{br, \lim} \quad (37)$$

$$P_{l,t}^{br} = \sum_{i=1}^{N_u} G_{l,i} P_{i,t}^{unit} - \sum_{j=1}^{N_L} G_{l,j} P_{j,t}^{load} \quad (38)$$

where  $P_{l,t}^{br}$  is the transmission power of branch  $l$  at time  $t$ ;  $P_{l,t}^{br, \lim}$  is the transmission power limit;  $G_{l,i}$  is the element of the transfer distribution factor matrix of the DC power flow, representing the impact of the injected power of node  $i$  on line  $l$ ;  $N_u$  is the number of various types of power unit;  $P_{i,t}^{unit}$  is the power output of unit  $i$  at time  $t$ ;  $N_L$  is the number of

load nodes; and  $P_{j,t}^{load}$  is the load demand of node  $j$  at time  $t$ .

The total generated power of various units in the EPS should be balanced with the load demand:

$$\sum_{i=1}^{I^{CHP}} P_{i,t}^{CHP} + \sum_{i=1}^{I^{CTP}} P_{i,t}^{CTP} + \sum_{i=1}^{I^{WP}} P_{i,t}^{WP} + \sum_{i=1}^{I^{PV}} P_{i,t}^{PV} = \sum_{i=1}^{I^{EB}} P_{i,t}^{EB} + P_t^{load} \quad (39)$$

where  $P_t^{load}$  is the EPS electric load at time  $t$ ;  $I^{CTP}$  is the number of the CTP units;  $I^{WP}$  is the number of wind turbines;  $I^{PV}$  is the number of photovoltaic units; and  $I^{EB}$  is the number of EBs.

The constraints of the PDR are defined in (15)-(23).

## 2) DHS

The extraction steam from the CHP unit is used for direct heating and heat storage. The heat transfer ratio links the extraction steam flow rate and the heat transfer power:

$$m_{i,t}^{CHP} = m_{i,t}^{dh} + m_{i,t}^{st} \quad (40)$$

$$H_{i,t}^{CHP} = H_{i,t}^{dh} + H_{i,t}^{st} \quad (41)$$

$$H_{i,t}^{dh} = k_i^{dh} m_{i,t}^{dh} \quad (42)$$

$$H_{i,t}^{st} = k_i^{st} m_{i,t}^{st} \quad (43)$$

where  $m_{i,t}^{dh}$  and  $m_{i,t}^{st}$  are the respective extraction steam flows for direct heating and heat storage, respectively;  $H_{i,t}^{dh}$  and  $H_{i,t}^{st}$  are the corresponding heat power; and  $k_i^{dh}$  and  $k_i^{st}$  are the heat transfer ratios that indicate the heat transfer capacity of the extraction steam for direct heating and heat storage, respectively.

Figure 7 shows that the heat source is composed of the CHP unit, the HSD, and the EB:

$$H_t^{hs} = \sum_{i=1}^{I^{CHP}} H_{i,t}^{dh} + \sum_{i=1}^{I^{HSD}} H_{i,t}^{rl} + \sum_{i=1}^{I^{EB}} H_{i,t}^{EB} \quad (44)$$

where  $H_t^{hs}$  is the thermal power entering the DHN at time  $t$ .

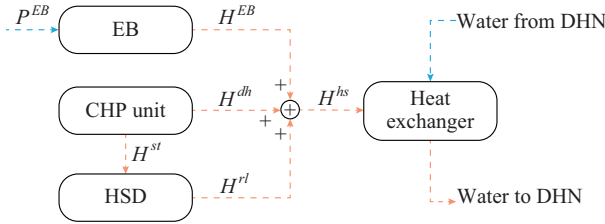


Fig. 7. Schematic of heat source.

A general pipeline transmission model [26] is used to describe the pipeline water flow. The average water temperature at the pipeline outlet can be expressed as a linear combination of the temperatures of two adjacent flow units:

$$T_{i,t}^{pipe,out} = aT_{i-k_1,t}^{pipe,in} + bT_{i-k_2,t}^{pipe,in} + cT^{soil} \quad (45)$$

where  $T_{i,t}^{pipe,out}$  is the pipe outlet average temperature at time  $t$ ;  $T_{i-k_1,t}^{pipe,in}$  and  $T_{i-k_2,t}^{pipe,in}$  are the pipe inlet temperatures at time  $(t-k_1)$  and  $(t-k_2)$ , respectively;  $k_1$ ,  $k_2$ , and the coefficients  $a$ ,  $b$ ,  $c$  are related to the parameters of the pipeline; and the product of the soil temperature  $T^{soil}$  and the coefficient  $c$  represents the heat loss caused by the heat exchange between the pipe and the outside.

The temperature mixing constraints of the pipeline node model are used to ensure energy conservation:

$$\sum_{i \in I_k^{pipe,in}} T_{i,t}^{pipe,out} m_{i,t}^{pipe} = \sum_{j \in I_k^{pipe,out}} T_{j,t}^{pipe,in} m_{j,t}^{pipe} \quad (46)$$

$$T_{m,t}^{pipe,in} = T_{n,t}^{pipe,in} \quad \forall m, n \in I_k^{pipe,out}, k \in I^{node} \quad (47)$$

where  $T_{i,t}^{pipe,out}$  and  $m_{i,t}^{pipe}$  are the outlet temperature and mass flow rate of pipeline  $i$  at time  $t$ , respectively;  $T_{j,t}^{pipe,in}$  and  $m_{j,t}^{pipe}$  are the inlet temperature and mass flow rate of pipeline  $j$  at time  $t$ , respectively;  $I_k^{pipe,out}$  and  $I_k^{pipe,in}$  are the outlet and inlet pipeline indices of node  $k$ , respectively; and  $I^{node}$  is the index set of nodes in the DHN.

The water outlet and inlet temperatures in the pipeline cannot exceed their upper and lower limits:

$$T_i^{pipe,min} \leq T_{i,t}^{pipe,out} \leq T_i^{pipe,max} \quad (48)$$

$$T_i^{pipe,min} \leq T_{i,t}^{pipe,in} \leq T_i^{pipe,max} \quad (49)$$

To ensure the thermal comfort of heat consumers, the equivalent buildings have the following constraints:

$$|T_{i,t+1}^b - T_{i,t}^b| \leq T_i^{ch} \quad (50)$$

$$|T_{i,t}^b - T_{i,t}^{com}| \leq T_i^{lim} \quad (51)$$

$$T_{i,t}^{com} = k_1^b T_{i,t}^{env} + k_2^b \quad (52)$$

$$\sum_{i=1}^N H_{i,t}^{br} \geq \sum_{i=1}^N \frac{T_{i,t}^{com} - T_{i,t}^{env}}{R_i^b} \quad (53)$$

where  $T_i^{ch}$  is the limit of temperature change in adjacent time;  $T_{i,t}^{com}$  is the thermal comfort temperature related to the outside temperature and correlation coefficients  $k_1^b$  and  $k_2^b$ ; and  $T_i^{lim}$  is the indoor temperature limit.

Other constraints of the DHS are mentioned in (1)-(14).

## C. Simulation Environment

As shown in Fig. 8, the optimal scheduling process of the IEHES model is an MILP problem. As an efficient mathematical programming solver developed by IBM, CPLEX is used to deal with various mathematical programming problems. In this paper, we use MATLAB and CPLEX to optimize the linear programming model. The software versions are IBM, ILOG, CPLEX, Optimizers 12.9.0, and MATLAB R2016a.

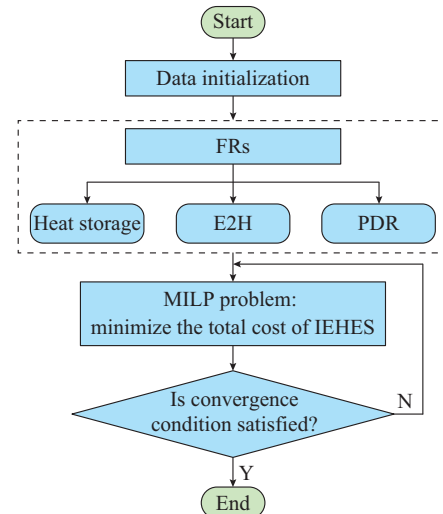


Fig. 8. Schematic of optimal scheduling process.

IV. CASE STUDY

A. Test Data and Cases

We choose a region in China for the simulation study. The electric load, outdoor temperature, and renewable energy output on a typical day are shown in Fig. 9. The optimal scheduling test system, including a 6-bus EPS and 6-node DHS, is shown in Fig. 10. The system has two CTP units (G1 and G2), a CHP unit, a wind farm, and a photovoltaic unit. The CHP unit and EB connect the EPS and the DHS, which, together with the HSD, form the heat source to provide heat to buildings. The detailed data of the test system come from [9], [26], [31]. We take 15 min as the period and 24 hours in a day as a complete scheduling time in the simulation. Furthermore, the total cost of IEHES dispatch is defined as the summation of 24 hours to ensure the optimal scheduling of the whole day.

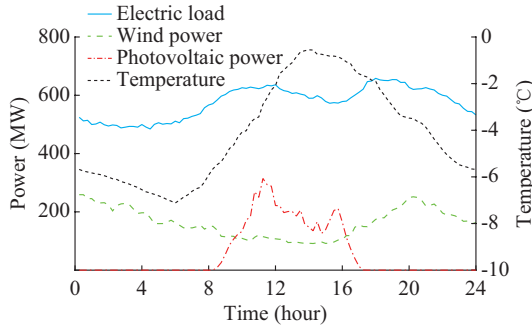


Fig. 9. Electric power and temperature curve on a typical day.

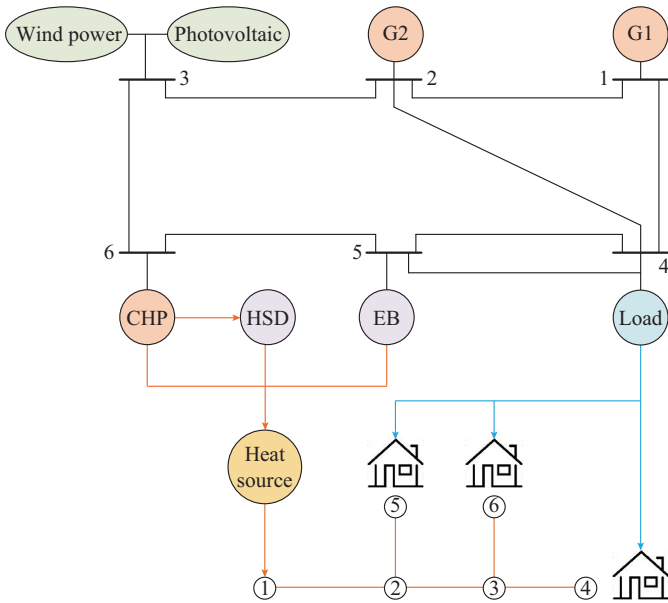


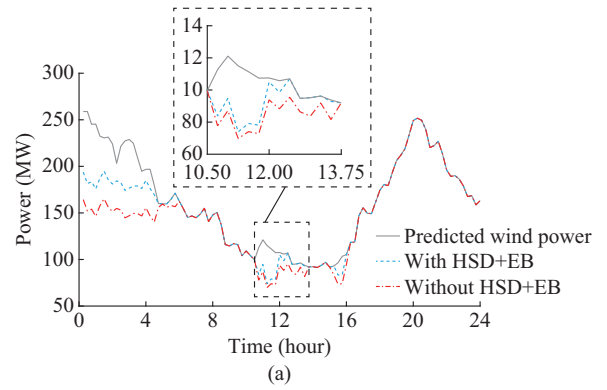
Fig. 10. Diagram of 6-bus EPS and 6-node DHS test system.

B. Separate Analysis of FRs

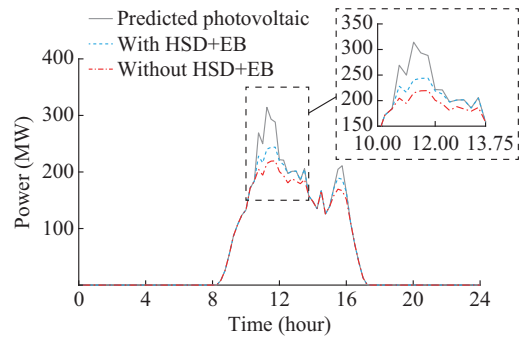
1) HSD and EB

The HSD and the EB are generally installed near the CHP unit to provide assisting heat source, and we combine the two for investigation. The renewable integration before and after configuration is shown in Fig. 11(a) and (b), respective-

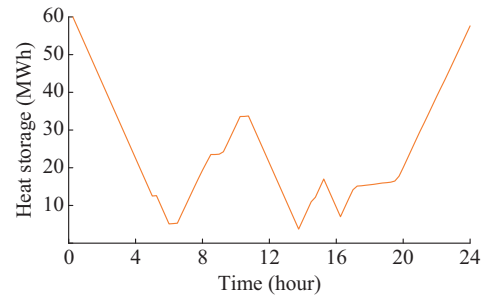
ly. The wind power curtailment occurs at 00:00-06:30 and 10:30-16:30, while the photovoltaic curtailment occurs at 10:30-16:30.



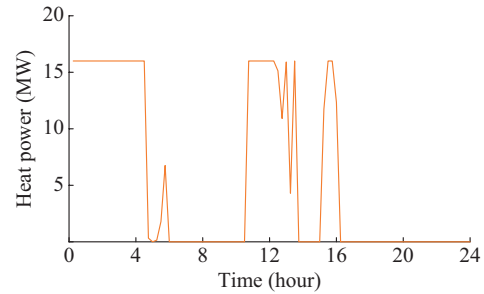
(a)



(b)



(c)



(d)

Fig. 11. Scheduling results with HSD and EB. (a) Wind power. (b) Photovoltaic. (c) Heat storage of HSD. (d) Heat power of EB.

Figure 11(c) and (d) shows the operation status of the HSD and the EB, respectively. The HSD releases stored heat and the EB performs electricity-heat conversion at 00:00-06:30. Similarly, at 10:30-16:30, the HSD and the EB work together to decouple the electrothermal restriction and integrate more renewable energy.

## 2) Thermal Inertia of DHS

As shown in Fig. 12(a) and (b), the IEHES accommodates more renewable energy after considering the thermal inertia of the DHS. The thermal inertia of the PHN is reflected in the inlet and outlet temperatures as shown in Fig. 12(c). At 00:00-06:30 and 10:30-16:30, the outlet temperature drops to release the heat stored in the PHN pipeline to prevent renewable curtailments from occurring. At other times, the pipeline temperature rises and the PHN stores heat. The thermal inertia of the equivalent building is reflected in the indoor temperature as shown in Fig. 12(d). Similar to the PHN pipeline, the thermal inertia of the buildings improves the flexibility of the IEHES.

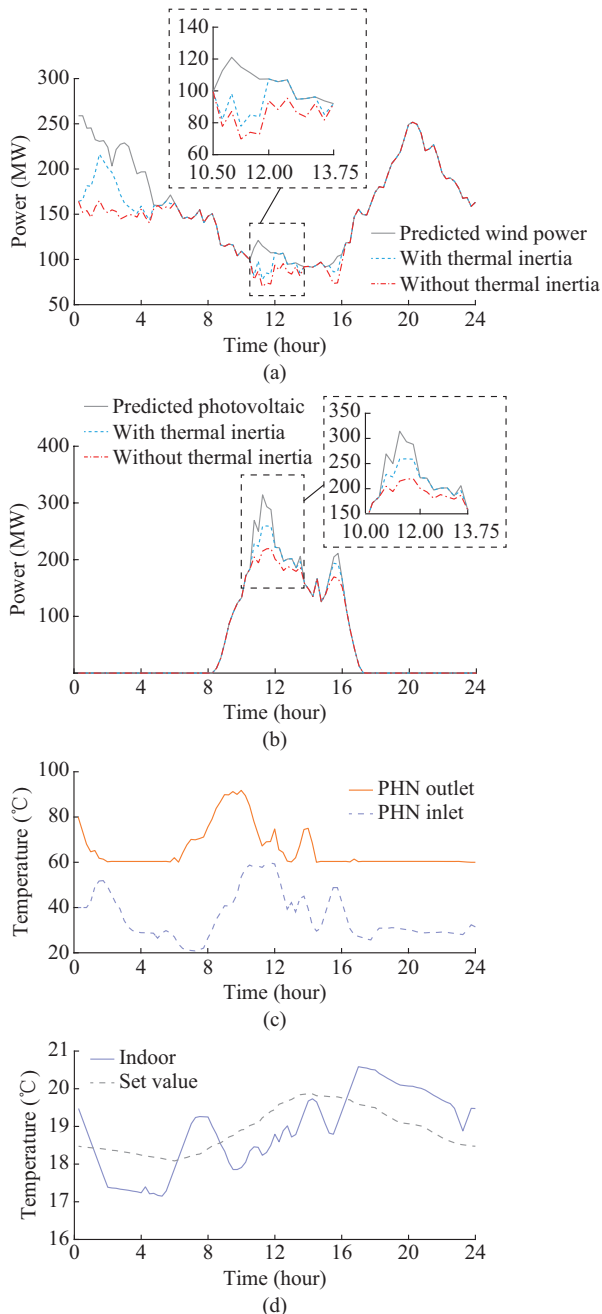


Fig. 12. Scheduling results with thermal inertia. (a) Wind power. (b) Photovoltaic. (c) PHN inlet and outlet temperatures. (d) Indoor temperature.

## 3) PDR

The PDR realizes synergy between the power supply and load demand through the shift of demand load. Figure 13(a) and (b) shows that PDR can effectively reduce renewable curtailments. The changes of the day-ahead electricity price and electric load are shown in Figs. 13(c) and (d), respectively. The electricity price drops in the period, which attracts more electric load to prevent renewable curtailments.

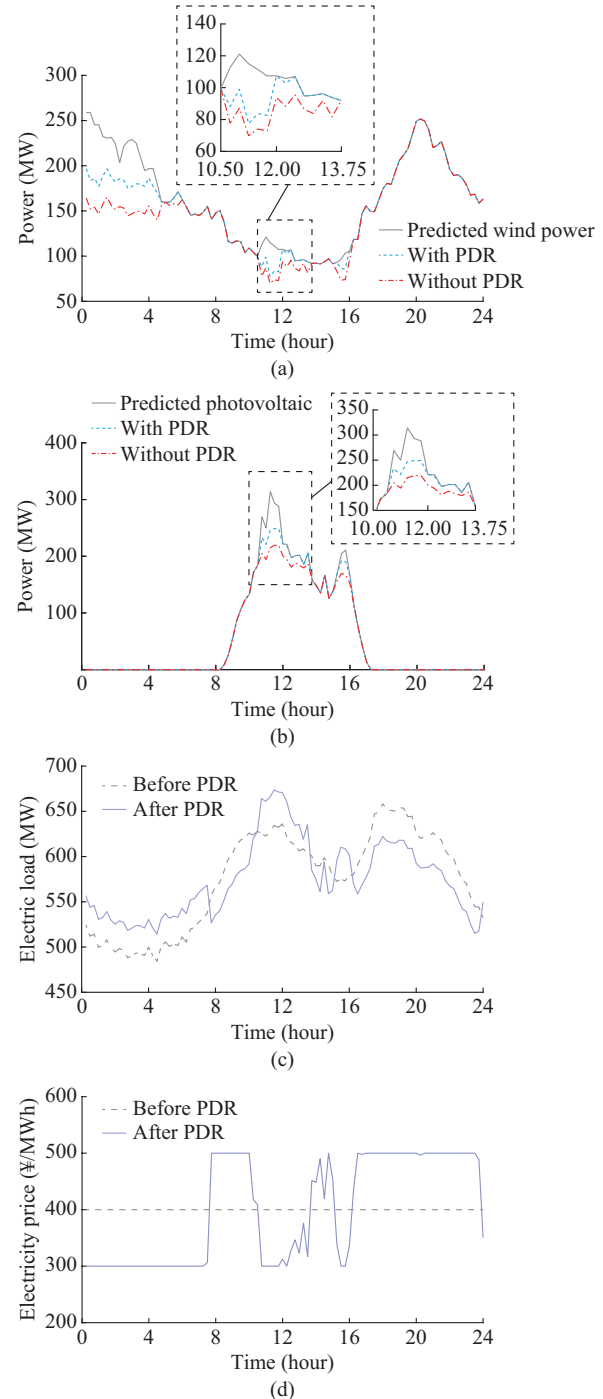


Fig. 13. Scheduling results with PDR. (a) Wind power. (b) Photovoltaic. (c) Electric load. (d) Day-ahead electricity price.

## 4) Contribution Degrees of FRs

The above simulation results indicate that the three types of FRs play an important role in reducing the curtailment of

renewable energy. The contribution degrees of different FRs are compared in Table I. The PDR has the best effect on increasing the wind power penetration and the curtailment is 221.9 MWh. The thermal inertia of DHS has the best effect on increasing the photovoltaic penetration and the curtailment is 56.4 MWh. Besides, PDR also reduces the total cost to a minimum of 3338.3 ton of standard coal equivalent (TCE). The analysis results have reference values for the selection and use of FRs.

TABLE I  
COMPARISON OF CONTRIBUTION DEGREE

FR	Total wind power curtailment (MWh)	Total photovoltaic curtailment (MWh)	Total cost (TCE)
None	410.6	147.2	3634.2
HSD+EB	236.4	73.4	3406.0
Thermal inertia	262.2	56.4	3363.7
PDR	221.9	63.4	3338.3

### C. Comprehensive Analysis

After separately discussing the operation and influence of flexible scheduling resources, we further analyze the combination method. Table II lists four cases for simulation testing, where the mark “√” means participating in scheduling and “/” is the opposite.

TABLE II  
OPTIMAL SCHEDULING CASES

Case	Heat source		DHS		EPS
	HSD	EB	PHN	Building	PDR
1	/	/	/	/	/
2	√	√	/	/	/
3	√	√	√	√	/
4	√	√	√	√	√

1) Case 1: reference case, where none of the FRs are considered.

2) Case 2: the HSD and the EB are considered on the heat source side.

3) Case 3: the HSD and the EB on the heat source side and the thermal inertia of DHS are all applied in scheduling.

4) Case 4: three types of FRs are considered.

Figure 14(a) and (b) indicates that the integration of renewable energy gradually increases with the addition of flexible scheduling resources. Figure 14(c) and (d) shows the fluctuation ranges of the CHP units, reflecting the improvement of system flexibility.

The total integrations of renewable energy and system cost in four cases are listed in Table III. A more detailed analysis is conducted based on these data. Figure 15(a) and (b) indicates that the renewable energy curtailment is gradually reduced with the addition of flexible scheduling resources. The wind power curtailment rate decreases from 10.5% in Case 1 to 1.4% in Case 4, and the photovoltaic curtailment rate decreases from 10.5% in Case 1 to 0.9% in Case 4. This result shows that renewable energy is almost completely integrated. Figure 15(c) reflects that the total cost re-

duction of the IEHES increases from 6.3% in Case 2 to 12% in Case 3, and then reaches 15.6% in Case 4 compared with Case 1. This indicates that the integration of renewable energy can also bring great benefits to electricity and heat productions.

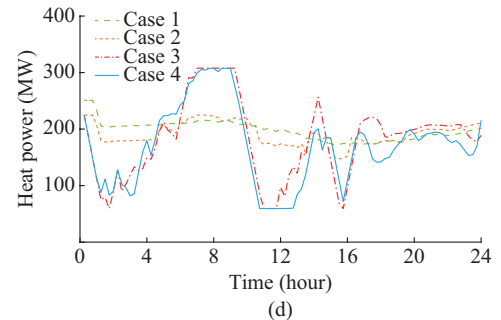
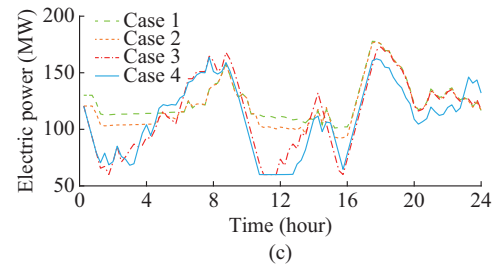
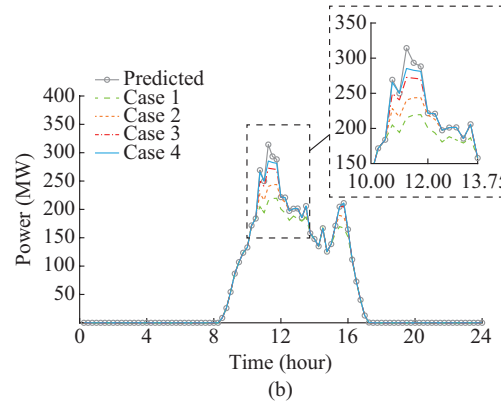
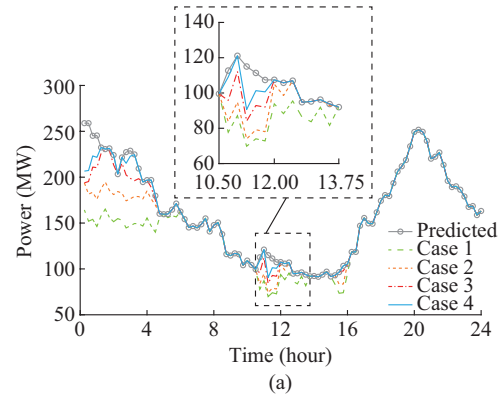


Fig. 14. Comparison of optimal scheduling results. (a) Wind power. (b) Photovoltaic. (c) Electric power of CHP unit. (d) Heat power of CHP unit.

### D. Simulations in Large System

As shown in Fig. 16, we perform the proposed method in a 30-bus and 12-node large system to illustrate the effectiveness and feasibility of the optimized scheduling strategy in the real dispatch process.

TABLE III  
RENEWABLE ENERGY INTEGRATION AND TOTAL COST

Case	Total wind power (MWh)	Total photovoltaic (MWh)	Total cost (TCE)
1	3498.0	1254.1	3634.2
2	3672.2	1327.9	3406.0
3	3801.8	1372.4	3198.9
4	3855.4	1388.7	3067.8

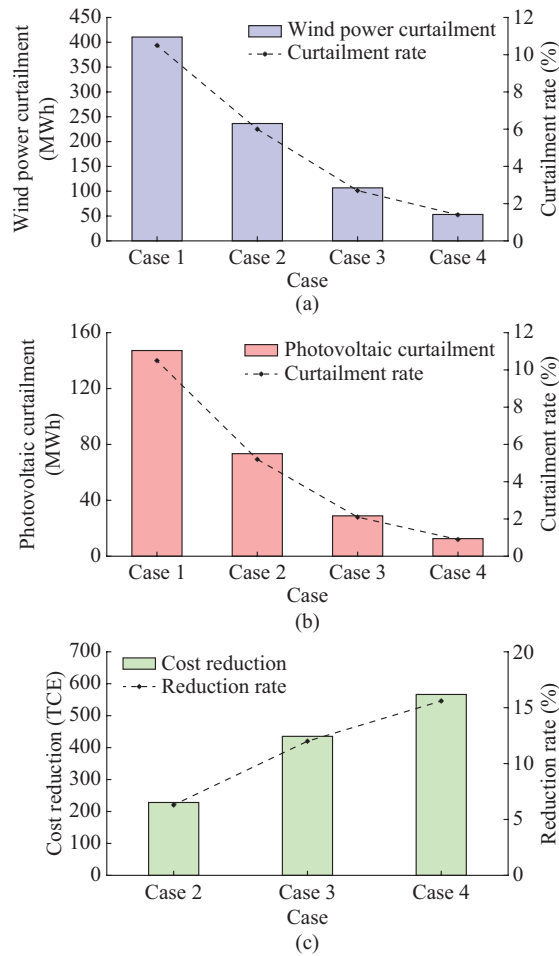


Fig. 15. Renewable energy curtailment and cost reduction. (a) Wind power curtailment. (b) Photovoltaic curtailment. (c) Cost reduction.

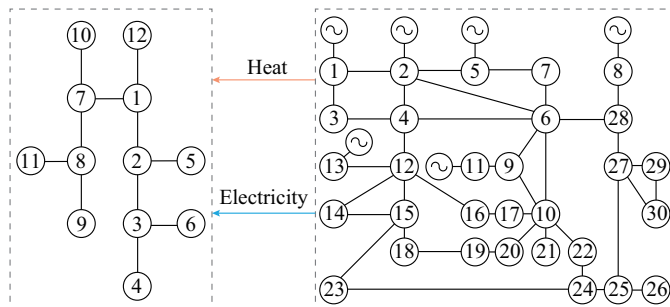


Fig. 16. Diagram of 30-bus and 12-node large system.

The 30-bus EPS consists of two CHP units, three CTP units, a wind farm, and a photovoltaic unit, which are locat-

ed at buses 1, 2, 5, 8, 11, 13. Two CHP units, 4 HSDs, and 4 EBs form the heat source for DHS heating. There are six buildings in the 12-node DHS serving as the thermal loads in the IEHES.

Similar to 6-bus and 6-node test system, we use the 4 cases listed in Table II for simulation. Figure 17(a) and (b) shows the integration results of wind power and photovoltaic. It can be observed that the renewable penetration is greatly improved with the addition of FRs, especially photovoltaics which basically achieves 100% consumption with all FRs. Besides, the data listed in Table IV also reflects the excellent effect of FRs on reducing the total costs of IEHES.

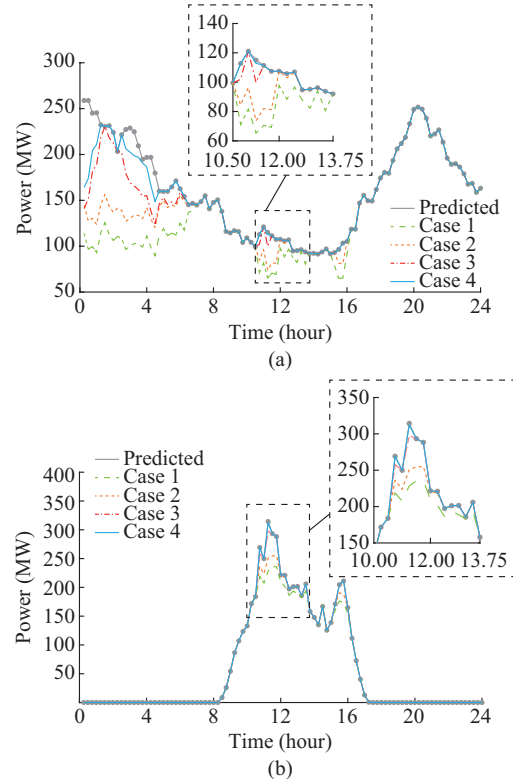


Fig. 17. Comparison of optimal scheduling results. (a) Wind power. (b) Photovoltaic.

TABLE IV  
RENEWABLE ENERGY INTEGRATION AND TOTAL COST

Case	Total wind power (MWh)	Total photovoltaic (MWh)	Total cost (TCE)
1	3196.8	1287.9	5891.8
2	3441.1	1342.7	5489.8
3	3678.3	1394.3	5149.5
4	3803.8	1400.8	5006.3

All the simulations are performed on a computer with Intel Core i7 CPU and 16 GB memory under MATLAB R2016a and CPLEX environment. The simulation times of the 4 cases in both systems are listed in Table V. The results indicate that the addition of FRs and the increase in system complexity both lead to an increase in simulation time, and the latter has a greater impact. Besides, even in the 30-bus and 12-node system with all FRs, the simulation time can be

controlled within about 3 minutes, which reflects the feasibility of the optimal dispatch method in real operation process.

TABLE V  
SIMULATION TIME OF 4 CASES

Case	Simulation time of 6-bus and 6-node system (s)	Simulation time of 30-bus and 12-node system (s)
1	18.28	88.03
2	19.40	135.66
3	22.39	161.89
4	29.30	181.08

## V. CONCLUSION

In this paper, FRs on the power supply and load sides of an IEHES are introduced to IEHES dispatch for renewable penetration. Three kinds of EHCRs and the SEDR are modeled in detail. The solution for FRs participating in IEHES dispatch is furthermore given, with goals of maximizing the renewable penetration ratio and lowering operation costs. A 6-bus EPS and 6-node DHS test system is tested, and the contribution degrees of different FRs for renewable integration are also explored. The results show that the renewable curtailments are nearly eliminated after introducing FRs: the wind power curtailment rate decreases from 10.5% to 1.4%, and the photovoltaic curtailment rate decreases from 10.5% to 0.9%. Furthermore, a 30-bus and 12-node system is performed, and the results prove the universality of the proposed approach in real applications. In future work, IEHES optimization considering electricity storage together with the orderly dispatch and management for different FRs will be explored.

## REFERENCES

- [1] X. Zhao, S. Zhang, R. Yang *et al.*, "Constraints on the effective utilization of wind power in China: an illustration from the northeast China grid," *Renewable & Sustainable Energy Reviews*, vol. 16, pp. 4508-4514, Sept. 2012.
- [2] R. Azizpanah-Abarghoee, T. Niknam, M. A. Bina *et al.*, "Coordination of combined heat and power-thermal-wind-photovoltaic units in economic load dispatch using chance-constrained and jointly distributed random variables methods," *Energy*, vol. 79, pp. 50-67, Jan. 2015.
- [3] China National Energy Administration. (2020, Oct.). Transcript of the online press conference of the National Energy Administration in the fourth quarter of 2020. [Online]. Available: [http://www.nea.gov.cn/202010/30/c\\_139478872.htm](http://www.nea.gov.cn/202010/30/c_139478872.htm)
- [4] H. Zhao, Q. Wu, S. Hu *et al.*, "Review of energy storage system for wind power integration support," *Applied Energy*, vol. 137, pp. 545-553, Jan. 2015.
- [5] X. Chen, M. B. McElroy, and C. Kang, "Integrated energy systems for higher wind penetration in China: formulation, implementation, and impacts," *IEEE Transactions on Power Systems*, vol. 33, no. 2, pp. 1309-1319, Mar. 2018.
- [6] G. Luo, Y. Li, W. Tang *et al.*, "Wind curtailment of China's wind power operation: evolution, causes and solutions," *Renewable & Sustainable Energy Reviews*, vol. 53, pp. 1190-1201, Jan. 2016.
- [7] A. Bloess, "Modeling of combined heat and power generation in the context of increasing renewable energy penetration," *Applied Energy*, vol. 267, p. 114727, Jun. 2020.
- [8] X. Guo, R. Gong, H. Bao *et al.*, "Hybrid stochastic and interval power flow considering uncertain wind power and photovoltaic power," *IEEE Access*, vol. 7, pp. 85090-85097, Jun. 2019.
- [9] X. Chen, C. Kang, M. O'Malley *et al.*, "Increasing the flexibility of combined heat and power for wind power integration in China: modeling and implications," *IEEE Transactions on Power Systems*, vol. 30, no. 4, pp. 1848-1857, Jul. 2015.
- [10] M. G. Nielsen, J. M. Morales, M. Zugno *et al.*, "Economic valuation of heat pumps and electric boilers in the Danish energy system," *Applied Energy*, vol. 167, pp. 189-200, Apr. 2016.
- [11] N. Zhang, X. Lu, M. B. McElroy *et al.*, "Reducing curtailment of wind electricity in China by employing electric boilers for heat and pumped hydro for energy storage," *Applied Energy*, vol. 184, pp. 987-994, Dec. 2016.
- [12] K. Hu, L. Chen, Q. Chen *et al.*, "Phase-change heat storage installation in combined heat and power plants for integration of renewable energy sources into power system," *Energy*, vol. 124, pp. 640-651, Apr. 2017.
- [13] Y. Teng, P. Sun, O. Leng *et al.*, "Optimal operation strategy for combined heat and power system based on solid electric thermal storage boiler and thermal inertia," *IEEE Access*, vol. 7, pp. 180761-180770, Dec. 2019.
- [14] B. Liu, J. Li, S. Zhang *et al.*, "Economic dispatch of combined heat and power energy systems using electric boiler to accommodate wind power," *IEEE Access*, vol. 8, pp. 41288-41297, Jan. 2020.
- [15] Z. Li, W. Wu, M. Shahidehpour *et al.*, "Combined heat and power dispatch considering pipeline energy storage of district heating network," *IEEE Transactions on Sustainable Energy*, vol. 7, no. 1, pp. 12-22, Jan. 2016.
- [16] Z. Li, W. Wu, J. Wang *et al.*, "Transmission-constrained unit commitment considering combined electricity and district heating networks," *IEEE Transactions on Sustainable Energy*, vol. 7, no. 2, pp. 480-492, Apr. 2016.
- [17] J. Huang, Z. Li, and Q. H. Wu, "Coordinated dispatch of electric power and district heating networks: a decentralized solution using optimality condition decomposition," *Applied Energy*, vol. 206, pp. 1508-1522, Nov. 2017.
- [18] C. Lin, W. Wu, B. Zhang, and Y. Sun, "Decentralized solution for combined heat and power dispatch through benders decomposition," *IEEE Transactions on Sustainable Energy*, vol. 8, no. 4, pp. 1361-1372, Oct. 2017.
- [19] J. Wang, Z. Zhou, J. Zhao *et al.*, "Improving wind power integration by a novel short-term dispatch model based on free heat storage and exhaust heat recycling," *Energy*, vol. 160, pp. 940-953, Oct. 2018.
- [20] S. Yao, W. Gu, S. Zhou *et al.*, "Hybrid timescale dispatch hierarchy for combined heat and power system considering the thermal inertia of heat sector," *IEEE Access*, vol. 6, pp. 63033-63044, Oct. 2018.
- [21] J. Zheng, Z. Zhou, J. Zhao *et al.*, "Effects of the operation regulation modes of district heating system on an integrated heat and power dispatch system for wind power integration," *Applied Energy*, vol. 230, pp. 1126-1139, Nov. 2018.
- [22] C. Wu, W. Gu, P. Jiang *et al.*, "Combined economic dispatch considering the time-delay of district heating network and multi-regional indoor temperature control," *IEEE Transactions on Sustainable Energy*, vol. 9, no. 1, pp. 118-127, Jan. 2018.
- [23] Z. Pan, Q. Guo, and H. Sun, "Feasible region method based integrated heat and electricity dispatch considering building thermal inertia," *Applied Energy*, vol. 192, pp. 395-407, Apr. 2017.
- [24] Y. Yang, K. Wu, H. Long *et al.*, "Integrated electricity and heating demand-side management for wind power integration in China," *Energy*, vol. 78, pp. 235-246, Dec. 2014.
- [25] K. Hedegaard and O. Balyk, "Energy system investment model incorporating heat pumps with thermal storage in buildings and buffer tanks," *Energy*, vol. 63, pp. 356-365, Dec. 2013.
- [26] Y. Dai, L. Chen, Y. Min *et al.*, "Dispatch model for CHP with pipeline and building thermal energy storage considering heat transfer process," *IEEE Transactions on Sustainable Energy*, vol. 10, no. 1, pp. 192-203, Jan. 2019.
- [27] Y. Dai, L. Chen, Y. Min *et al.*, "Integrated dispatch model for combined heat and power plant with phase-change thermal energy storage considering heat transfer process," *IEEE Transactions on Sustainable Energy*, vol. 9, no. 3, pp. 1234-1243, Jul. 2018.
- [28] Y. Dai, L. Chen, Y. Min *et al.*, "A general model for thermal energy storage in combined heat and power dispatch considering heat transfer constraints," *IEEE Transactions on Sustainable Energy*, vol. 9, no. 4, pp. 1518-1528, Oct. 2018.
- [29] Y. Dai, L. Chen, Y. Min *et al.*, "Active and passive thermal energy storage in combined heat and power plants to promote wind power accommodation," *Journal of Energy Engineering*, vol. 143, no. 5, pp. 1-15, Oct. 2017.
- [30] L. Mitridati, J. Kazempour, and P. Pinson, "Heat and electricity market coordination: a scalable complementarity approach," *European Journal of Operational Research*, vol. 283, no. 3, pp. 1107-1123, Jun.

- 2020.
- [31] M. I. Alomoush, "Optimal combined heat and power economic dispatch using stochastic fractal search algorithm," *Journal of Modern Power Systems and Clean Energy*, vol. 8, no. 2, pp. 276-286, Mar. 2020.
- [32] T. Shekari, A. Gholami, and F. Aminifar, "Optimal energy management in multi-carrier microgrids: an MILP approach," *Journal of Modern Power Systems and Clean Energy*, vol. 7, no. 4, pp. 876-886, Jul. 2019.
- [33] D. S. Kirschen, G. Strbac, P. Cumperayot *et al.*, "Factoring the elasticity of demand in electricity price," *IEEE Transactions on Power Systems*, vol. 15, no. 2, pp. 612-617, May. 2000.
- [34] L. A. Greening, "Demand response resources: who is responsible for implementation in a deregulated market?" *Energy*, vol. 35, no. 4, pp. 1518-1525, Apr. 2010.
- [35] C. Zhao, J. Wang, J.-P. Watson *et al.*, "Multi-stage robust unit commitment considering wind and demand response uncertainties," *IEEE Transactions on Power Systems*, vol. 28, no. 3, pp. 2708-2717, Aug. 2013.
- [36] Z. Tan, L. Ju, B. Reed *et al.*, "The optimization model for multi-type customers assisting wind power consumption considering uncertainty and demand response based on robust stochastic theory," *Energy Conversion and Management*, vol. 105, pp. 1070-1081, Nov. 2015.
- [37] N. Lu, "An Evaluation of the HVAC load potential for providing load balancing service," *IEEE Transactions on Smart Grid*, vol. 3, no. 3, pp. 1263-1270, Sept. 2012.
- [38] Q. Chen, R. Fu, and Y. Xu, "Electrical circuit analogy for heat transfer analysis and optimization in heat exchanger networks," *Applied Energy*, vol. 139, pp. 81-92, Feb. 2015.
- [39] Y. Zhou, W. Hu, Y. Min *et al.*, "Integrated power and heat dispatch considering available reserve of combined heat and power units," *IEEE Transactions on Sustainable Energy*, vol. 10, no. 3, pp. 1300-1310, Jul. 2019.

**Wei Wang** received the Ph.D. degree in control theory and control engineering from North China Electric Power University, Beijing, China, in 2011. He is now an Associate Professor with the State Key Laboratory of Alter-

nate Electrical Power System with Renewable Energy Sources, North China Electric Power University. His research interests mainly include the modeling, optimization and control of integrated energy system.

**Shuhao Huang** received the B.Sc. degree in School of Control and Computer Engineering from North China Electric Power University, Beijing, China, in 2018. He is currently pursuing his M.S. degree in control theory and control engineering at North China Electric Power University. His research interests include modeling, optimization, and control of integrated energy system.

**Guangming Zhang** received the M.Eng. degree in School of Control and Computer Engineering from North China Electric Power University, Beijing, China, in 2018. He is currently pursuing his Ph.D. degree in control theory and control engineering at North China Electric Power University. His research interests include modeling, optimization, and control of integrated energy system.

**Jizhen Liu** received the M.S. degree in power plant engineering from Graduate Faculty of North China Electric Power Institute, Beijing, China, in 1982. He is now an Academician of China Academy of Engineering, and a Professor with the State Key Laboratory of Alternate Electrical Power System with Renewable Energy Sources, North China Electric Power University. His research interests include large-scale renewable energy integration.

**Zhe Chen** received the B.Eng. and M.Sc. degrees in electrical engineering from Northeast China Institute of Electric Power Engineering, Jilin, China, in 1982 and 1986, respectively, and the Ph.D. degree in electrical engineering from the University of Durham, Durham, UK, 1997. He is a Full Professor with the Department of Energy Technology, Aalborg University, Aalborg, Denmark. He is a Leader of Wind Power System Research Program with the Department of Energy Technology, Aalborg University, and the Danish Principal Investigator for Wind Energy of Sino-Danish Centre for Education and Research. He has led many research projects and has more than 500 publications in his technical fields. His research areas are power systems, power electronics and electric machines, and his main current research interests include wind energy and modern power systems.